American Mineralogist, Volume 92, pages 631–639, 2007

Anomalous behavior at the *I*2/*a* to *Imab* phase transition in SiO_2-moganite: An analysis using hard-mode Raman spectroscopy

Peter J. Heaney,[1,*] David A. McKeown,[2] and Jeffrey E. Post[3]

[1]Department of Geosciences, 309 Deike, Penn State University, University Park, Pennsylvania 16802, U.S.A.
[2]Vitreous State Laboratory, Catholic University of America, 620 Michigan Avenue, NE, Washington, D.C. 20064, U.S.A.
[3]Department of Mineral Sciences, National Museum of Natural History, Smithsonian Institution, Washington, D.C. 20560-0119, U.S.A.

Abstract

The silica polymorph moganite is commonly intergrown with quartz in microcrystalline silica varieties that are less than ~100 Ma in age. Synchrotron X-ray diffraction suggests that a displacive phase transition occurs when moganite is heated above ~570 K, with an increase in symmetry from *I*2/*a* to *Imab*. In the present study, we employed hard-mode Raman spectroscopy to confirm the existence of the α-β moganite transformation and to offer complementary insight into the transition mechanism. Our analysis of the displacement of the 501 Δcm^{-1} symmetric stretching-bending vibration (B_{3g} mode) with changing temperature strongly supports the existence of a monoclinic-to-orthorhombic phase transition between 570 and 590 K. Between 593 and 723 K, however, the mode remained fixed at 496 Δcm^{-1}. This behavior was repeated on cooling, but with a hysteresis of over 100 K. We offer three hypotheses that may explain this observation: (1) the intergrowth of nanoscale quartz lamellae within moganite may exert a strain that inhibits the transition; (2) the transition may exhibit a martensitic character marked by the co-existence of α- and β-moganite over a finite temperature interval; and (3) the α- and β-moganite transition may occur via an intermediate phase.

Keywords: Moganite, phase transition, Raman spectroscopy, silica

Introduction

Moganite has received less scientific scrutiny than its polymorphic brethren in the silica family because it passed virtually unrecognized until Flörke and colleagues reported its existence within rhyolitic ignimbrites from Gran Canaria, Spain, 30 years ago (Flörke et al. 1976, 1984). More recently, the determination of its structure (Miehe et al. 1988; Miehe and Graetsch 1992) and the discovery of its abundance in most microcrystalline "quartz" varieties (Heaney and Post 1992), have established both the validity of moganite and its importance as a distinct silica phase. Analyses of such silica varieties as chert, flint, chalcedony, and agate from around the world reveal that most of these materials crystallize with between 5 and 20 wt% moganite (Heaney and Post 1992). Consequently, the International Mineralogical Association's Commission on New Minerals and Mineral Names (CNMMN) approved moganite as a mineral species in 1999. In this paper, we explore the high-temperature behavior of moganite using in situ Raman microprobe spectroscopy.

No evidence to date suggests that moganite occupies a stability field within the pure SiO_2 system, and the diversity of environments in which moganite occurs is sufficiently large that the factors that favor its formation still are poorly understood. Moganite appears to be strictly a low-pressure crustal mineral, and it apparently does not exhibit a pressure-induced transition to another crystalline phase. Diamond-anvil-cell studies document a progressive amorphization of moganite up to 25 GPa (Léger 2001). In low-pressure regimes, moganite precipitates from fluids that range from room temperature to several hundred degrees Celsius. Heaney (1995) argued that higher moganite concentrations are diagnostic of evaporitic silica deposits, and subsequent studies have substantiated the observation that surficial brines precipitate a significant fraction of moganite along with quartz within microcrystalline silcretes and playa sediments (Bustillo 2001; English 2001; Nash and Hopkinson 2004).

Recent research has demonstrated that moganite also is a common mineral in hydrothermal environments. Parthasarathy et al. (2001) reported that hydrothermal chalcedony nodules within the gas cavities of the Deccan flood basalts in Maharastra, India typically contain 70 ± 10 wt% moganite. These nodules rival the chert seams in Gran Canaria, the type locality for moganite, in their moganite abundance. In addition, Rodgers and coworkers (Herdianita et al. 2000; Rodgers and Cressey 2001; Rodgers and Hampton 2003; Hampton et al. 2004) have shown that moganite is a typical intermediate phase in the diagenesis of geothermal opal-A to quartz. These authors examined microcrystalline quartz-bearing sinters from 13 active and extinct geothermal systems over a range of localities in New Zealand, and they documented the presence of moganite at levels of up to ~13 wt% in samples between 20 000 and 200 000 years in age. With longer maturation times, the concentration of moganite in these sinters decreases as larger fractions of moganite have transformed to quartz. Similarly, moganite is observed as an intermediate phase in the diagenesis of permineralized fossil wood (Witke et al. 2004). The observation that moganite is a metastable transitory phase during silica diagenesis supports inferences presented in Heaney and Post (1992) and Moxon and Ríos (2004), who discerned no moganite in microcrystalline "quartz" varieties older than the Devonian.

* E-mail: heaney@geosc.psu.edu

0003-004X/07/0004–631$05.00/DOI: 10.2138/am.2007.2184

The precipitation of moganite not only in low-temperature evaporitic brines but also in silica-rich, hot waters in natural environments warrants an exploration of its thermal behavior. The highest temperature at which moganite will precipitate from aqueous fluids is not known, as a method for the synthesis of moganite has yet to be reported. Nevertheless, Hopkinson et al. (1999) have identified moganite within chalcedony from hydrothermal submarine vents in the mid-Atlantic, and they infer an upper limit of ~633 K for chalcedony crystallization in these smokers. Moreover, the solubility of moganite as a function of temperature is of broad significance for its bearing on the proper application of the "chalcedony geothermometer," which uses dissolved silica concentrations in hydrothermal fluids as a proxy for temperature (Fournier and Rowe 1966; Fournier 1977). Gíslason et al. (1997) have shown that, at room temperature, the solubility of moganite (44 mg/kg) is significantly greater than that of quartz (6 mg/kg). Therefore, the solubility of a given chalcedony specimen is intrinsically related to its moganite/quartz ratio.

Interestingly, the solubilities for moganite measured by Gíslason et al. (1997) exhibited a decreasing temperature dependence with increased heating. At 473 K (the highest temperature in their study), the change in solubility appears to plateau as a function of temperature, and the difference in solubility between moganite and quartz is significantly diminished (Fig. 1). An extrapolation of the moganite solubility data to higher temperatures suggests that moganite and quartz solubilities become equal between 523 and 573 K. This dramatic decrease in the sensitivity of moganite solubility to temperature may be related to a structural transition. Based on temperature-resolved synchrotron XRD experiments, Heaney and Post (2001) proposed that at 573 K, moganite experiences a displacive phase transformation that leads to an expanded framework above the transition point. The transformation entails an increase in symmetry from space group *I*2/*a* to *Imab*, and it is reversible on cooling.

The present study is an effort to confirm the occurrence of a phase transition between monoclinic α-moganite and orthorhombic β-moganite at ~573 K using temperature-resolved, hard-mode Raman spectroscopy, and to search for structural anomalies at the transition, as are observed in the other low-pressure polymorphs of silica (quartz, tridymite, and cristobalite) (reviewed in Heaney 1994). Raman spectroscopy is ideally complementary to XRD for studies of moganite/quartz intergrowths because the technique probes over shorter distances than does XRD (reviewed in McMillan and Hofmeister 1988). This difference in the characteristic length scales of the two methods leads to subtle disparities in measurements of the same physical properties, such as the moganite/quartz ratio (Götze et al. 1998). Nevertheless, because Raman spectra of moganite are distinct from those of quartz (Kingma and Hemley 1994), the method has become a common approach for the non-destructive identification of moganite in microcrystalline silica samples (e.g., Rodgers and Hampton 2003; Nash and Hopkinson 2004; Witke et al. 2004). As the present study demonstrates, Raman spectroscopy also proves more effective than XRD for monitoring certain aspects of thermally induced structural transitions in moganite.

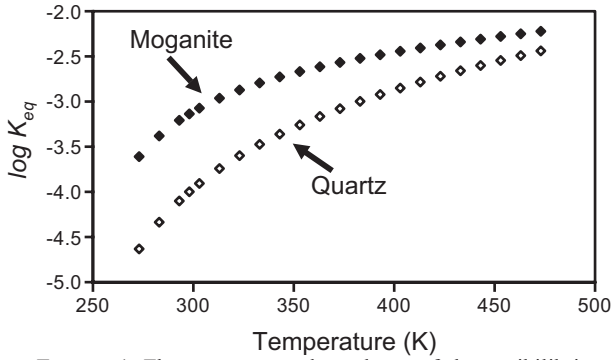

FIGURE 1. The temperature dependence of the equibilibrium constants for the hydrolysis of moganite and quartz. From Table 6 of Gíslason et al. (1997).

EXPERIMENTAL METHODS

The samples used in this study were chert nodules from the ignimbrites of the Mogán D formation near the town of Mogán, Gran Canaria, Spain. Singly polished petrographic thin sections measuring 30 μm in thickness were prepared from several different nodules using a soluble adhesive. The chert wafers were removed from the glass slide mounts for Raman data collection. Raman measurements were made using fragments from these wafers, including both translucent chert cores with ~50 wt% moganite and opaque white inclusions with upward of 70 wt% moganite, as was ascertained separately by powder XRD. The mixed moganite/quartz Raman spectra collected from these specimens matched closely those presented in Kingma and Hemley (1994). Two fragments were selected for high-temperature heating experiments on the basis of high moganite content, peak sharpness, and good peak-to-background contrast. For purposes of comparison, Raman and XRD data were collected from a sample of pure powdered quartz from Hot Springs, Arkansas.

For each run, the moganite fragment was placed in a small Pt crucible within a TS1500 heating stage, supplied by Linkam. Before heating experiments were initiated, the sample was annealed at 673 K for 10 min to volatilize loosely sorbed water and to minimize "false" hysteresis effects by mobilizing defects and dislocations. Heating experiments were performed in air, with a ceramic heat shield placed over the crucible within the ceramic heating block. The sample then was heated at a rate of 100 K/min from room temperature to 473 K, 50 K/min to 543 K, and 20 K/min at temperatures above 543 K. Spectra were collected at 373, 473, 523, and 543 K, and then at 10 K increments up to 603 K, and beyond 623 K at 50 K increments up to a maximum temperature of 873 K. To ensure thermal equilibrium for the sample, the stage was maintained at each temperature for at least 1 minute before any spectrum was collected. The sample then was cooled in the reverse temperature order, while using the same rates outlined above. Under identical conditions, the heating-stage thermocouple was temperature calibrated by performing melting runs each for KNO_3 (T_f = 606 K), Na_2SO_4 (T_f = 1157 K), and $NaSiO_3$ (T_f = 1361 K). Temperatures reported for the moganite heating experiments were corrected using the resultant calibration curve, so that the reported temperatures are within ±4 K of the actual temperature.

Parallel-polarized Raman spectra were gathered using a notch filter single-grating spectrograph system (Goncharov and Struzhkin 2003). An EXEL Model 3000 Ar^+ laser provided the 457.9 nm wavelength incident light that was directed to the optical microscope that guided the laser light down to the sample surface through a long-working-distance 10× microscope objective. The laser light passed through the silica glass window of the heating stage, through the 1 mm diameter hole in the heat shield, and was focused to a 10 μm diameter spot on to the fragment. The laser power was approximately 20 mW at the sample. The spectra were gathered in back-scattering geometry, where the scattered light was directed back through the heating-stage window and an analyzer polarizer in the microscope column.

After the analyzer, the scattered light proceeded through holographic notch and super-notch filters (Kaiser Optical Systems), which reduced the Rayleigh scattered light intensity by 10 optical densities. The notch filters were oriented in the scattered light path so that the filter cut-off in the collected spectra was near 60 Δcm^{-1} from the laser line. The incident slits of the spectrograph (JY-Horiba HR460) were set to 6 cm^{-1} resolution. The spectrograph used a 1200 gr/mm grating (Richardson Grating Laboratory) that was set to 480.50 nm to disperse the Stokes scattered light from the sample onto a 2048 × 512-element Peltier-cooled CCD detector (Model DU440BV from Andor Technology). The spectrograph was frequency calibrated using a Ne lamp and CCl_4, so that the recorded frequencies are accurate to within ±1 cm^{-1}. The 298 K Raman spectra were collected with the sample in the heating stage but without the silica window in the incident and scattered light path.

All spectra collected at temperatures above 298 K were obtained with the silica glass window in place. Each spectrum collected was an average of 10 accumulations, collected at 10 seconds each. All spectra were corrected for notch-filter, grating-efficiency, and detector-quantum-efficiency effects on the scattered light intensities. Notch-filter corrections were effective down to near 100 Δcm^{-1}; Raman intensities of features below 100 Δcm^{-1} in the spectra presented are probably distorted. The presence of the heating-stage window in the incident and scattered light paths caused a 0.4 Δcm^{-1} frequency shift in the resulting spectra, which was later corrected.

Raman spectra were fit using the program IGOR v. 4.06 Carbon, written by WaveMetrics. Peaks at 450 and 501 Δcm^{-1} were fit using 3 Lorentzian functions, of which one modeled the background and the other 2 fit the Raman mode peaks.

Results and discussion

Raman spectra at room temperature

Raman spectra for pure quartz and for moganite-rich chert are presented in Figure 2. As can be seen in this figure (and in the study of Kingma and Hemley 1994), quartz and moganite exhibit several similar vibrational modes, although the peaks generated by the moganite-rich chert generally are broader than those in the quartz spectrum. The correspondence in the spectra of quartz and moganite is not surprising since the two phases share structural motifs that are closely related (Fig. 3). Miehe and Graetsch (1992) described moganite as quartz that is Brazil twinned along (101) at the unit-cell scale. Specifically, slabs of right-handed, quartz-like structure alternate regularly with slabs of left-handed quartz to generate a doubled superperiodicity along <101>* relative to the quartz structural end-member. In a complementary view, the structures of quartz and moganite are seen to be constructed from linear tetrahedral chains (parallel to [110] in quartz and [010] in moganite) that are connected via isolated bridging tetrahedra. The topological disparity between the two structures (and the concomitant variation in handedness) is tied to the locations of the bridging tetrahedra relative to the linear chains to which they are bonded (Heaney 1993). The space group for moganite is monoclinic (*I2/a*) rather than trigonal ($P3_221$ or $P3_121$), as is observed for α-quartz.

The most notable departure of the Raman spectrum for moganite in comparison with that of quartz is observed in the frequencies of their most intense bands (Fig. 2). In quartz, the highest intensity mode occurs at 465 Δcm^{-1}, whereas in moganite, it is found at 501 Δcm^{-1}. Moganite also exhibits a relatively intense band at 463 Δcm^{-1} that overlaps the major 465 Δcm^{-1} mode of quartz, but the 501 Δcm^{-1} peak for moganite suffers from minimal interference. Diagnostic bands for quartz and moganite also are observed in the low-frequency portions of the spectrum (at 207 Δcm^{-1} for quartz and 220 Δcm^{-1} for moganite), and some authors have made use of these modes to discriminate between quartz and moganite in siliceous sinters (e.g., Rodgers and Cressey 2001). The broadness of the 220 Δcm^{-1} line in moganite, however, renders it unsuitable for high-temperature spectroscopic analysis, as additional broadening occurs on heating.

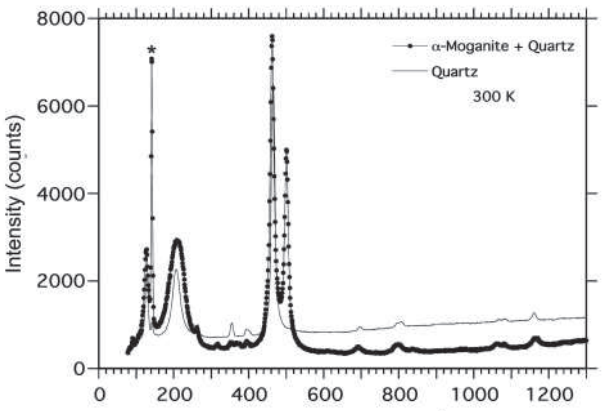

Figure 2. Raman spectra for pure quartz and for a mixture of moganite and quartz at room temperature. Peaks arising from Raman shifts associated with water vapor molecules are labeled with an asterisk.

No evidence for soft mode

Displacive phase transitions typically are associated with the freezing-in of a specific high-temperature vibrational mode when crystals are cooled to a critical temperature. Below this temperature, atomic restoring forces are sufficiently strong to maintain the bonds that characterize the low-temperature twin configurations, despite thermally induced atomic displacements.

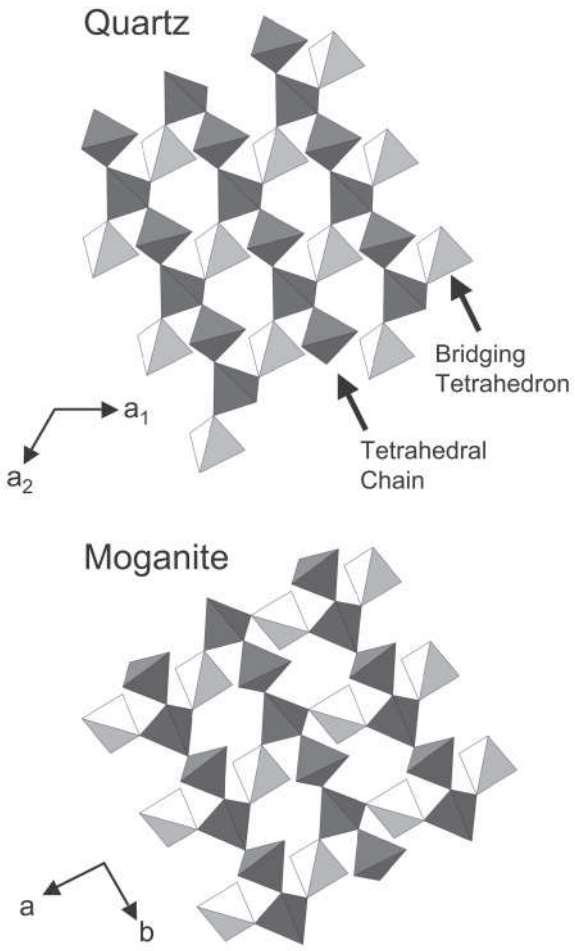

Figure 3. Projections of portions of the quartz and moganite structures along their **c**-axes. Linear tetrahedral chains along [110] in quartz and [010] in moganite are darkly tinted, and bridging tetrahedra are lighter.

As a crystal is heated near the critical temperature, however, these restoring forces weaken dramatically, and the vibrational modes related to these forces broaden, decrease in intensity, and approach zero frequency. The α-β quartz transition was the first solid-state transformation that yielded evidence for such soft modes (Landsberg and Mandelstam 1929; Raman and Nedungadi 1940), and in quartz it is the 207 Δcm^{-1} vibration that was thought to disappear completely above the α-β quartz transition temperature (T_{tr}) of 846 K.

It now is recognized that when quartz is heated, this 207 Δcm^{-1} mode decreases in frequency and exchanges positions with a two-phonon transverse acoustic (TA_1) mode at 147 Δcm^{-1} (Shapiro et al. 1967; Scott 1968; Berge et al. 1984). Close to T_{tr}, the frequency of the two-phonon mode increases to near 160 Δcm^{-1}, whereas the frequency of the soft mode diminishes to 30 Δcm^{-1} (Dolino and Vallade 1994). Tucker et al. (2000) argued that this soft mode remains a very low frequency rigid unit mode (RUM) in β-quartz, which is characterized by extreme orientational disorder of the silica tetrahedra due to the excitation of the soft mode and the other RUMs.

Although the 220 Δcm^{-1} mode in moganite has been inferred to correspond to the 207 Δcm^{-1} mode in quartz (Kingma and Hemley 1994), our heating experiments did not support its assignment as a soft mode in moganite. The 220 Δcm^{-1} peak broadened with increasing temperature, but it retained its relatively high intensity even when the sample was heated above the α-β moganite transition temperature of ~573 K. In fact, the 220 Δcm^{-1} mode persisted above the α-β quartz transition temperature of 846 K. It is not a surprise that the structural transformation that attends the α-β quartz transition is not manifested in moganite. The tetrahedral rotations that relate the two Dauphiné twin orientations in α-quartz are incompatible with the Brazil twin boundary structure in quartz; the tetrahedral vibrations associated with the soft mode in quartz would sever Si-O bonds located along a boundary that separates regions of opposite chirality. As evidence, dark-field transmission electron microscopy of amethyst at temperatures near 846 K demonstrates that the dynamical Dauphiné microtwin walls do not transect or interact with the Brazil twin boundaries (Van Goethem et al. 1977). Since the moganite structure can be modeled as quartz that is Brazil-twinned at the unit-cell scale, the rigid unit modes that attend the α-β quartz transition are not expected to have identical vibrational analogs in moganite.

Consequently, our high-temperature Raman experiments have not yet yielded information concerning soft-mode behavior in moganite. The displacive quality of the transition, as described in Heaney and Post (2001), suggests that such a mode must exist. Our failure to observe the mode in this study may be attributed to several factors: (1) the intensity of the peak may have been too low to be discriminated from the background; (2) the mode may overlap stronger peaks; or (3) the mode may occur at a frequency that lies below the lower limit of the collection range in this study (60 Δcm^{-1}).

Hard-mode analysis

Background. Although Raman analyses of displacive phase transformations conventionally focus on the soft modes associated with the transition, it increasingly is recognized that the temperature dependence of hard-mode parameters can offer important insights into transition behavior (reviewed in Bismayer 2000). Changes in crystal structure inevitably alter vibrational character, and Raman spectroscopy is particularly sensitive to the local structural environment due to the short correlation lengths of high-frequency phonons (Salje 1992). We selected the 501 cm^{-1} Raman vibrational mode for moganite to study, because it is the most intense and has minimal interference from quartz.

Raman spectra for a heating run from RT to 873 K and over the frequency range of 420 to 540 Δcm^{-1} are shown in Figure 4. A dashed line indicates the shifting position of the 501 Δcm^{-1} vibrational peak. The temperature dependencies of the frequency and peak width of this 501 Δcm^{-1} mode are presented in Figures 5 and 6, respectively. It can be seen from the figures that the mode softened slightly and broadened with higher temperature; by 873 K, the mode frequency had decreased to 494 Δcm^{-1}, and the peak width nearly doubled from 12 to 23 Δcm^{-1} between RT and 873 K. Reproducible anomalies in the variation of the 501 Δcm^{-1} peak parameters as a function of temperature support the proposed

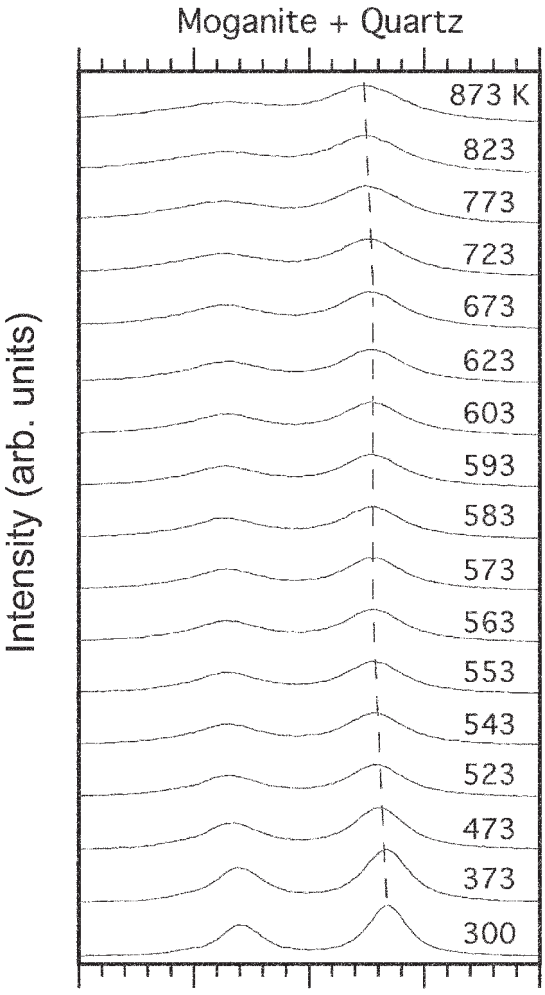

Figure 4. Raman spectra for a moganite/quartz mixture with increasing temperature. The dashed line connects peak maxima for the 501 Δcm^{-1} mode in moganite. View at low angle to observe anomalous peak behavior at the transition.

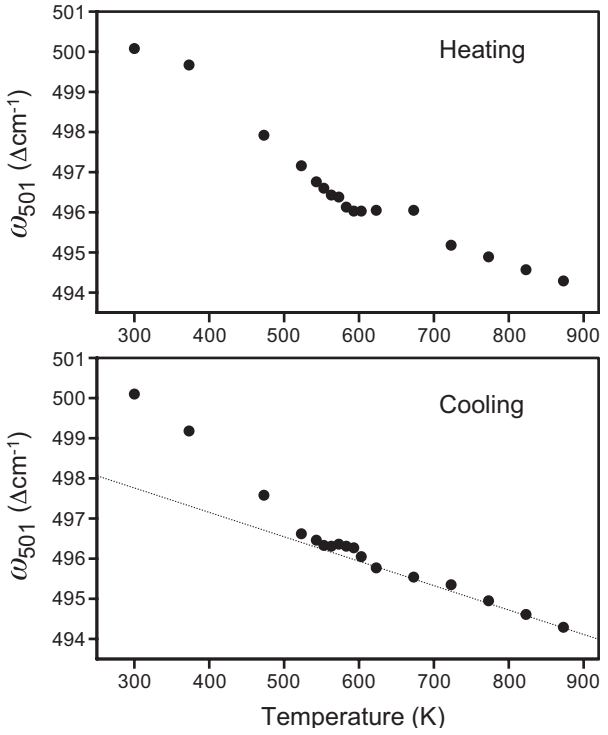

FIGURE 5. The temperature dependence of the 501 Δcm^{-1} vibrational frequency for heating (top) and cooling (bottom) cycles of moganite. The dashed line represents frequencies that are derived from a linear least-squares fit of β-moganite parameters and extrapolated into the stability field for α-moganite.

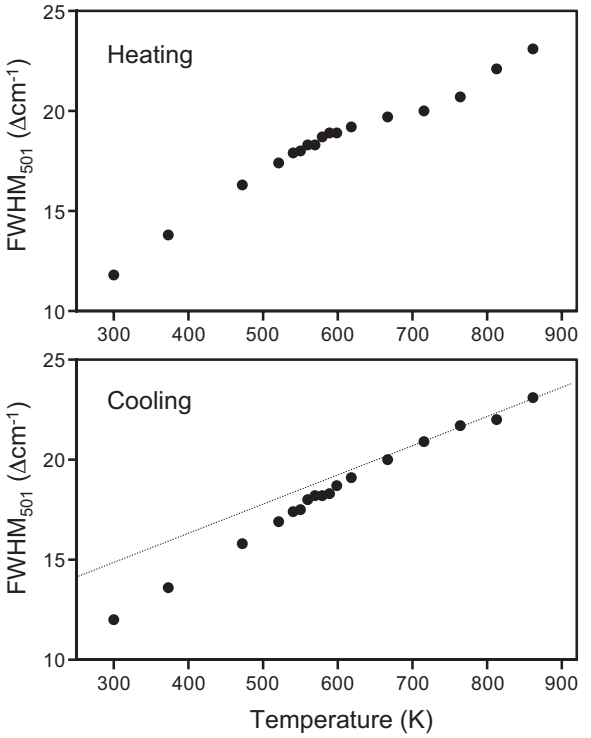

FIGURE 6. The temperature dependence of the full-width at half-maxima (FWHM) for the 501 Δcm^{-1} mode for heating (top) and cooling (bottom) cycles of moganite. The dashed line represents frequencies that are derived from a linear least-squares fit of β-moganite parameters and extrapolated into the stability field for α-moganite.

existence of an *I2/a*-*Imab* phase transition in moganite.

Evidence for a phase transition. In our experiments, the frequency of the 501 Δcm^{-1} mode decreased as a function of temperature from RT to 593 K, at which point it remained fixed (within error) at 496 Δcm^{-1} up to a temperature of 723 K (Fig. 5). With further heating, the frequency resumed its softening, but with a smaller temperature dependence than in the first stage of heating. On cooling, this same frequency-vs.-temperature dependence of the 501 Δcm^{-1} mode was repeated; from 873 to 593 K, the frequency increased from 494 to 496 Δcm^{-1}; the peak then remained at constant frequency until further cooling to 543 K. Below this temperature, the frequency increased to its initial starting value at RT but with a stronger temperature dependence than was observed at high temperature. Consequently, changes in slope of the 501 Δcm^{-1} peak frequency as a function of temperature (i.e., changes in $d\omega/dT_{501}$ where ω represents units of relative wavenumbers) were observed during both heating and cooling cycles, but the temperature at which the slopes changed was characterized by a hysteresis of 130 K. Analogous behavior was observed in the temperature dependence of the 501 Δcm^{-1} peak width (Fig. 6), as measured by its full width at half maximum (FWHM$_{501}$).

A change in the value of $d\omega/dT$ for hard modes at the critical temperature is characteristic of phase transitions, and thus the variations observed for the 501 Δcm^{-1} peak strongly support the structural transition in moganite proposed by Heaney and Post (2001). The inversion from α-moganite with space group *I2/a* to β-moganite with space group *Imab* is associated with the Brillouin zone center. An analysis of the non-symmetry breaking elastic (ε_{nsb}) and volume (V_s) strains as a function of temperature led these researchers to conclude that the transition is second order ($Q^2 \propto T \propto \varepsilon_{nsb} \propto V_s$, where Q is the order parameter). The behavior of hard modes in the Raman spectra should express the second-order character in an analogous fashion. The square of the order parameter is expected to vary linearly with the spontaneous vibrational displacement ($\Delta\omega$) for hard modes (Carpenter and Salje 1998). This parameter was measured by extrapolating through the values of the observed 501 Δcm^{-1} frequency shift in β-moganite into the stability field for α-moganite, and then by taking the difference between the observed and extrapolated values for ω_{501} in the low-temperature phase. The spontaneous vibrational broadening (FWHM) is measured in a similar way and also is expected to vary linearly with the square of the order parameter. Consequently, both $\Delta\omega_{501}$ and FWHM$_{501}$ should exhibit a linear thermal dependence through the relationship of temperature with the order parameter ($Q^2 \propto T \propto \Delta\omega \propto \Delta$FWHM).

For moganite, the dependencies of $\Delta\omega_{501}$ and ΔFWHM$_{501}$ on temperature are seen in Figure 7, based on data obtained during the cooling experiments. As would be expected of a second-order transition, both $\Delta\omega_{501}$ and ΔFWHM$_{501}$ varied linearly with temperature, with correlation coefficients (r^2) of 0.986 and 0.975, respectively. These calculations excluded those data over the intermediate temperature intervals for which the mode

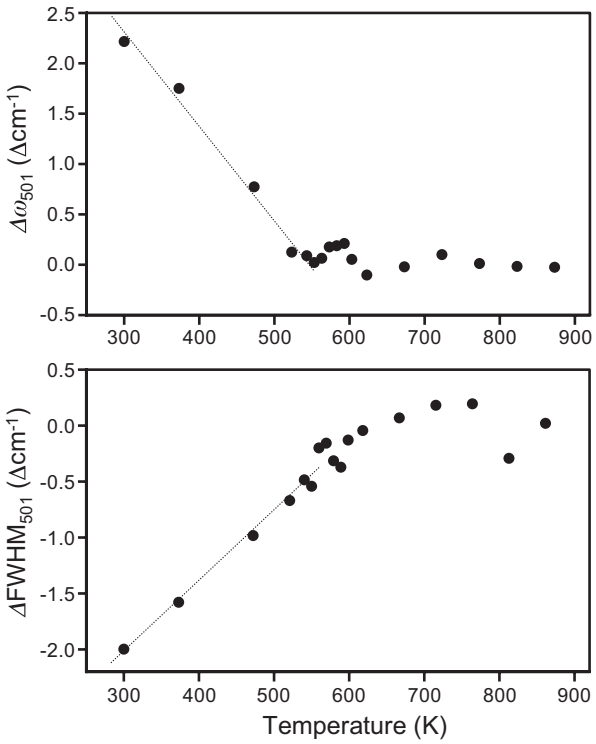

FIGURE 7. Variations in the departures of the frequency (top) and the full-width at half-maxima from their extrapolated values based on the thermal dependence of these parameters in β-moganite.

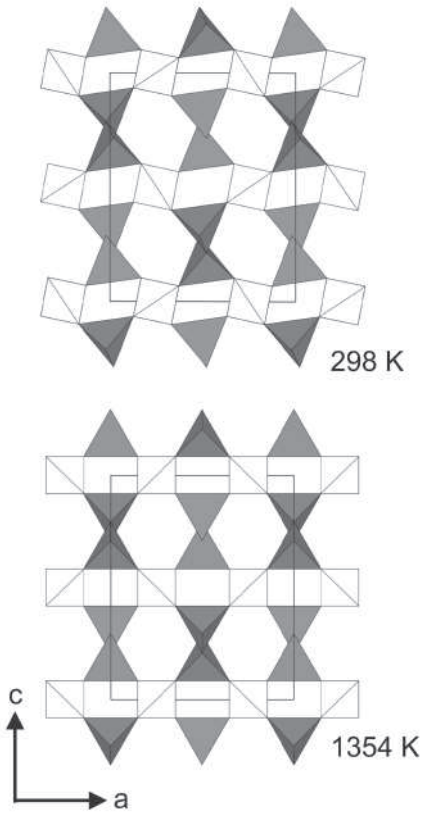

FIGURE 8. Projections of the structures of α-moganite at RT (top) and β-moganite at 1354 K (bottom). The transition from the low- to the high-temperature polymorph is effected by rotations of bridging Si1 tetrahedra (light) about the ***b***-axis.

remained pinned to 496 Δcm^{-1}, and thus they represent the relationship between α- and β-moganite. Although these results are concordant with the powder XRD analysis of Heaney and Post (2001), the possible existence of an intermediate phase and the hysteresis associated with the transition temperature are more commonly expected of a first-order transition. A determination of the nature of the intermediate structure may help to resolve this apparent inconsistency.

Structure of β-moganite. The model for the α-β moganite phase transition proposed in Heaney and Post (2001) involves a rotation about the ***a***-axis of the [010] linear tetrahedral chains and a rotation about the ***b***-axis of the so-called bridging tetrahedra (see Fig. 3). The net result of these combined motions is a dramatic expansion of the structure along the ***a***-axis when moganite is heated to T_{tr}, at which point the bridging tetrahedra are fully rotated, and the open tunnels parallel to ***b*** have evolved from rhombic to rectangular in cross section (Fig. 8). The linear [010] tetrahedral chains remain kinked at T_{tr}, and continued rotation of these chain tetrahedra about the ***a***-axis above T_{tr} leads to a progressive extension of the structure along ***b***. Consequently, the unit-cell volume of moganite continues to increase above the α-β moganite transition temperature, in contrast to quartz, which actually experiences a slight unit-cell volume decrease above the α-β phase transition (Carpenter et al. 1998). The thermally induced changes in the moganite ***a***-axis and in the unit-cell volumes for moganite and quartz, when normalized to the same number of molecular SiO_2 units, are represented in Figure 9.

Raman spectra above and below the moganite transition temperature are shown in Figure 10 for a quartz/moganite mixture, which contained 35 wt% quartz and 65 wt% moganite, as ascertained by Rietveld refinement of the bulk material. For both the α- and β-moganite structures, the correlation method (Fateley et al. 1972) predicts 51 optical modes, where 27 are Raman-active. Raman-active vibrational species include $13A_g + 14B_g$ modes for α-moganite, and $7A_g + 6B_{1g} + 6B_{2g} + 8B_{3g}$ modes for β-moganite. Therefore, theory predicts no change in the number of observed Raman modes for the α- and β-moganite transition, as is seen in Figure 10.

Raman mode frequencies were calculated for the moganite structure at 300 and 582 K using a simple two-force constant valence potential model (Dowty 1987), where the force constant values were varied to minimize the difference between observed mode frequencies (taken from the spectra) and calculated mode frequencies. Weak intensities and the broad widths of many peaks, as well as possible overlap from quartz peaks, rendered the assignment of some observed peak frequencies difficult, especially for β-moganite. The lattice-dynamics program (Dowty 1987) minimized the average deviation between observed and calculated mode frequencies to 7.4 Δcm^{-1} for the 300 K structure and 6.8 Δcm^{-1} for the 582 K structure. Consequently, the calculation described most of the moganite-related features in the spectra quite well (Fig. 10). In Figure 10, a question mark was

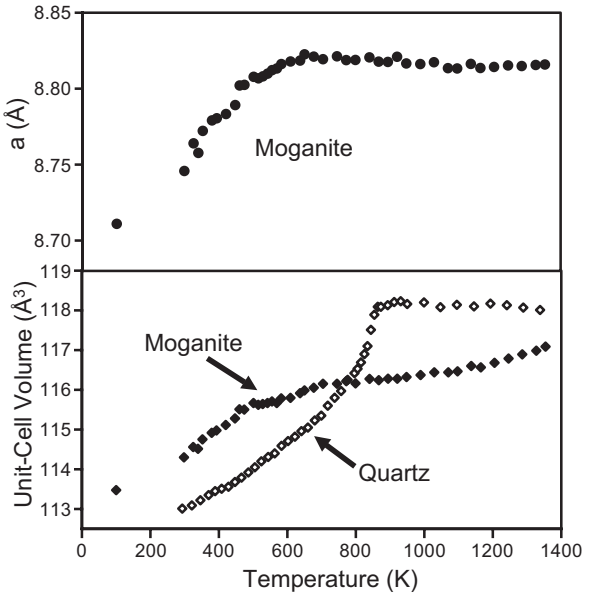

FIGURE 9. The temperature dependence of the unit-cell volume of moganite and quartz when volume is normalized to the same number of molecular SiO_2 units. Moganite data from Heaney and Post (2001), and quartz data are from Carpenter et al. (1998).

placed above each calculated mode that could not be clearly assigned to a specific spectral feature; these unassigned calculated modes did not have an observed frequency value for refinement and were not included in the average deviation calculation. The two force constants used for each structure were refined to reasonable values (compared with the lattice-dynamics results for other silicate structures in McKeown et al. 1995 and McKeown 2005), where $k_{Si\text{-}O} = 4.42 \times 10^5$ dyne/cm at 300 K and 4.30×10^5 dyne/cm at 582 K, and $k_{O\text{-}Si\text{-}O} = 2.79 \times 10^{-11}$ erg at 300 K and 2.70×10^{-11} erg at 582 K. The calculated 515 Δcm^{-1} B_{3g} mode most closely corresponds to the observed 501 Δcm^{-1} mode at room temperature, and the atomic displacement vectors associated with this mode are depicted in Figure 11.

Nature of the intermediate structure. Perhaps the most surprising observation in our Raman analysis of the moganite phase transition involved the behavior of the 501 Δcm^{-1} mode slightly above the transition temperature. For both heating and cooling cycles, the vibrational frequency remained constant at 496 Δcm^{-1} once the transition temperature was achieved, until a sufficiently large degree of overheating (or undercooling) forced the structural transformation to proceed. The temperature interval over which the mode was stationary was 130 K (between 593 and 723 K) on heating but only 50 K (from 593 to 543 K) on cooling. This hysteresis occurred despite our efforts to mobilize point defects, which might have been pinning twin boundaries and dislocations, through preliminary cycling of the samples through T_{tr} to 673 K and holding at this temperature for 10 min.

We can propose three possible explanations for the observed behavior:

(1) The intimate intergrowth of moganite with quartz in the powders that we studied may have exerted a constraining effect that inhibited the transformation. Transmission electron microscopy of these powders (Heaney and Post 1992) has revealed that

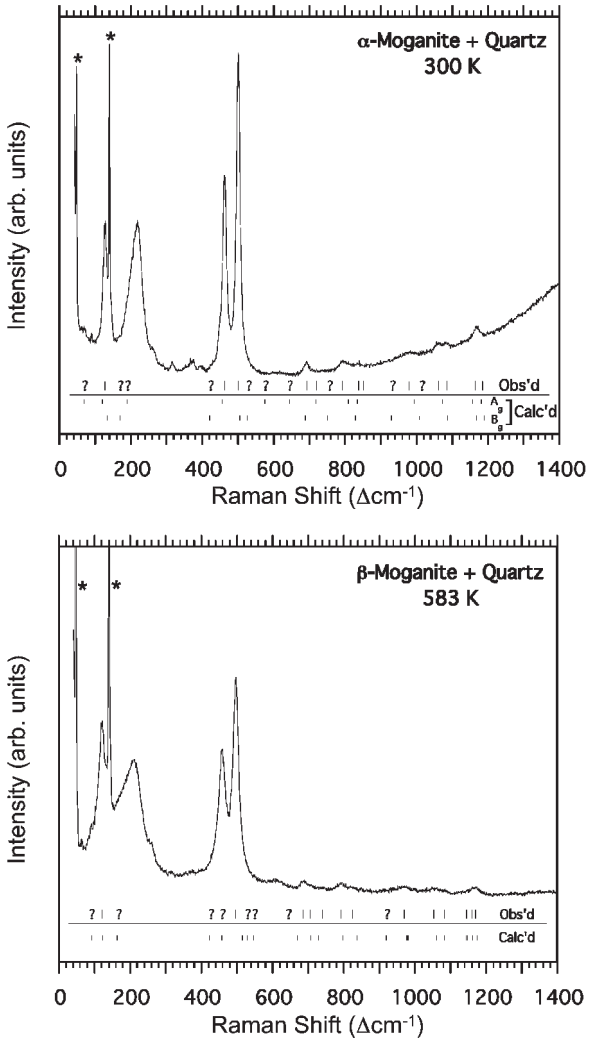

FIGURE 10. Raman spectra for a moganite/quartz mixture at 27 °C (**top**) and 309 °C (**bottom**) with observed and calculated vibrational mode frequencies indicated. Peaks arising from Raman shifts associated with water vapor molecules are labeled with an asterisk. A question mark is placed above each calculated mode that could not be clearly assigned to a specific moganite spectral feature.

the effective particle size of moganite is on the order of tens of nanometers because of the intercalation of structural packets with the same chirality (i.e., quartz). Consequently, the thermal independence of the 501 Δcm^{-1} mode near T_{tr} may reflect the suppression of the transition due to nanoscale particle sizes. For example, Ríos et al. (2001) have shown that the first-order character at the α-β quartz transition is strongly reduced in agates; the surface relaxation of the nanocrystals in agate exert an elastic clamping effect that dramatically renormalizes the fourth-order term in the Landau potential for the quartz phase transition. On the other hand, in powder XRD analyses of moganite (Heaney and Post 2001), the [010] tetrahedral chains continuously rotated when heated through the transition, leading to a gradual increase of the ***b***-axis. At the length scale probed by X-rays, therefore, there was no indication of an interruption in the volume expansion through the transition point. We also note that the sample

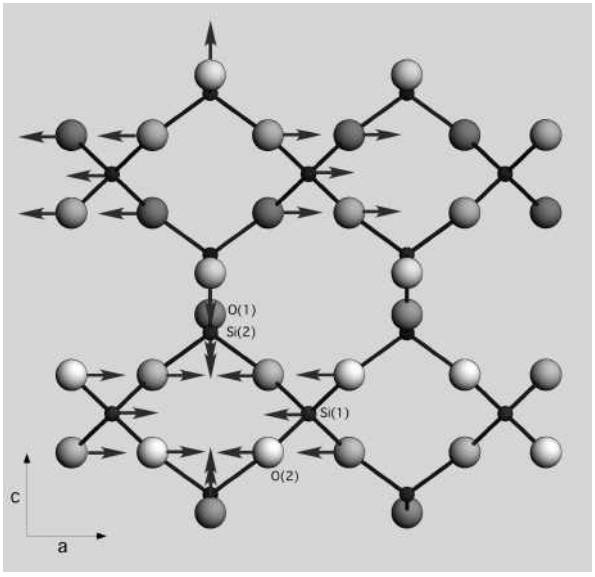

FIGURE 11. Modeled atomic vibration directions for the B_{3g} mode, calculated at 515 Δcm^{-1} and corresponding to the observed mode at 501 Δcm^{-1}.

deterioration that prevented the inclusion of cooling data in the nanoquartz study of Ríos et al. (2001) was not evident in our investigations of moganite.

(2) Moganite may transform via a martensitic mechanism. The transition temperature between the low ($P4_12_12$) and high ($Fd\bar{3}m$) modifications of cristobalite is marked by a hysteresis as large as 40 K (Phadke and Kshirsagar 1986), and powder XRD and differential scanning calorimetry (Leadbetter and Wright 1976; Schmahl 1993) have revealed that the hysteresis does not reflect limited reaction rates. Rather, when α-cristobalite transforms to β-cristobalite (typically between 500 to 550 K), the two polymorphs coexist over a 20 K interval. This behavior is repeated on cooling, and sustained heating at a constant temperature within the 20 K window does not induce a change in the degree of transformation. This athermal transition behavior is reminiscent of martensitic transformations in metals, and Schmahl (1993) argued that the hysteresis arises from coherency strain at the interface between α- and β-cristobalite.

The hysteresis observed at the α-β moganite transformation similarly might arise from a coexistence of the high- and low-temperature modifications over a finite transition interval. Weighing against this interpretation is the much smaller volume strain in moganite in comparison with that of cristobalite. The coherency strain that underlies the martensitic quality of the cristobalite transition arises from the enormously large difference in unit-cell volumes of the low and high modifications. The value of V_s at $T/T_{tr} = 0.5$ in cristobalite is slightly greater than 5% (Schmahl et al. 1992), whereas the half-transition volume strain in moganite is only ~1% (Heaney and Post 2001). Consequently, the degree of structural distortion over the moganite transition is relatively small. Moreover, Swainson et al. (2003) have examined several IR- and Raman-active hard modes in cristobalite as a function of temperature, and they did not report a temperature independence near T_{tr} for any vibrational modes in cristobalite of the kind observed in our study of the 501 Δcm^{-1} mode in moganite.

(3) The α-β moganite transition may be characterized by an intermediate phase. It is well established that the inversion from the low- to high-modifications of quartz is attended by an incommensurate phase that is stable over a 1.3 K interval and consists of ordered arrays of Dauphiné microtwins (reviewed in Heaney and Veblen 1991). Likewise, as tridymite is heated from room temperature and transforms to the so-called "HP" polymorph (with space group $P6_3/mmc$) at ~653 K, it undergoes a complex series of transformations, one of which involves the so-called OS phase, which is stable between 423 and 473 K. OS-tridymite exhibits an incommensurately modulated superperiodicity primarily along the ***a***-axis of the orthorhombic cell (Nukui et al. 1979; Graetsch and Brunelli 2005).

Since these other two low-pressure polymorphs of silica pass through intermediate phases in their march toward their high-temperature aristotypes, it is possible that moganite shares in this behavior. The search for satellite reflections that would be diagnostic of an incommensurate phase in moganite at T_{tr} was unsuccessful because of the large peak widths and high backgrounds associated with the powder XRD patterns of natural moganite. Several parameters in our previous XRD experiments suggest that the onset of the transition in moganite occurs near 590 K; this is the point at which the value of the ***a***-axis reaches a plateau and the cell angle β equals 90° in the Rietveld analysis of powder diffraction data (Heaney and Post 2001). It also was the temperature at which $\delta\omega/\delta T$ for the 501 Δcm^{-1} mode went to zero in the Raman experiments described here. It is interesting that the change in the thermal dependence of unit-cell volume occurs at a substantially lower temperature, closer to 500 K (Fig. 9). This behavior may provide some diffraction evidence for the kinds of structural anomalies that might accompany an intermediate phase. Ultimately, resolution of this issue may require the discovery or synthesis of single crystals of moganite that are large enough for crystallographic or spectroscopic analyses that are unfettered by quartz intergrowths.

CONCLUDING REMARKS

Hard-mode Raman spectroscopy of moganite as a function of temperature strongly supports the identification of an $I2/a$ to $Imab$ phase transition at ~590 K, as was suggested by a prior powder X-ray diffraction study (Heaney and Post 2001). The transformation involves cooperative tilting operations of two symmetrically distinct tetrahedra. The so-called bridging tetrahedra (Si1 in Heaney and Post 2001) rotate about the *b*-axis, and this motion is accompanied by a rotation about *a* of the [010] linear chains (Si2 in Heaney and Post 2001). Similar to the other low-pressure polymorphs of silica (quartz, tridymite, and cristobalite), moganite displayed anomalous behavior at its transition. The softening of the 501 Δcm^{-1} mode on heating ceased over a 130 K temperature interval, and this behavior was reproduced with a hysteresis on cooling. The reason for this arrested softening remains unclear, but further exploration of this transition is warranted because recent studies have demonstrated that moganite can form in geothermal fluids that are hotter than the transition temperature. Consequently, natural moganite in

hydrothermal environments will pass through the phase transition on cooling, and the attendant transition effects (e.g., the formation of twins) can strongly affect the physical properties of moganite, such as solubility.

ACKNOWLEDGMENTS

This work was supported by National Science Foundation grant no. EAR04-17714. This manuscript was greatly improved by the comments of two anonymous reviewers and by the editorial handling of Jill Pasteris. We are grateful to Michael Carpenter for insightful discussions on Landau analysis.

REFERENCES CITED

Berge, B., Vallade, M., and Martinez, G. (1984) Raman scattering investigation of the α–β transition and of the incommensurate phase in quartz. Journal of Physics C: Solid State Physics, 17, L167–L171.

Bismayer, U. (2000) Hard mode spectroscopy of phase transitions. In S.A.T. Redfern and M.A. Carpenter, Eds., Transformation Processes In Minerals, 39, p. 265–283. Reviews in Mineralogy and Geochemistry, Mineralogical Society of America, Chantilly, Virginia.

Bustillo, M.A. (2001) Cherts with moganite in continental Mg-clay deposits: An example of "false" Magadi-type cherts, Madrid Basin, Spain. Journal of Sedimentary Research, 71, 436–443.

Carpenter, M.A. and Salje, E.K.H. (1998) Elastic anomalies in minerals due to structural phase transitions. European Journal of Mineralogy, 10, 693–812.

Carpenter, M.A., Salje, E.K.H., Graeme-Barber, A., Wruck, B., Dove, M.T., and Knight, K.S. (1998) Calibration of excess thermodynamic properties and elastic constant variations associated with the α ↔ β phase transition in quartz. American Mineralogist, 83, 2–22.

Dolino, G. and Vallade, M. (1994) Lattice dynamical behavior of anhydrous silica. In P.J. Heaney, C.T. Prewitt, and G.V. Gibbs, Eds., Silica: Physical Behavior, Geochemistry, and Materials Applications, 29, p. 403–431. Reviews in Mineralogy, Mineralogical Society of America, Chantilly, Virginia.

Dowty, E. (1987) Fully automated microcomputer calculation of vibrational spectra. Physics and Chemistry of Minerals, 14, 67–79.

English, P.M. (2001) Formation of analcime and moganite at Lake Lewis, central Australia: Significance of groundwater evolution in diagenesis. Sedimentary Geology, 143, 219–244.

Fateley, W.G., Dollish, F.R., McDevitt, N.T., and Bentley, F.F. (1972) Infrared and Raman Selection Rules for Molecular and Lattice Vibrations: the Correlation Method. Wiley, New York.

Flörke, O.W., Jones, J.B., and Schmincke, H.-U. (1976) A new microcrystalline silica from Gran Canaria. Zeitschrift für Kristallographie, 143, 156–165.

Flörke, O.W., Flörke, U., and Giese, U. (1984) Moganite: a new microcrystalline silica-mineral. Neues Jahrbuch für Mineralogie. Abhandlungen, 149, 325–336.

Fournier, R.O. (1977) Chemical geothermometers and mixing models for geothermal systems. Geothermics, 5, 41–51

Fournier, R.O. and Rowe, J.J. (1966) Estimation of underground temperatures from the silica content of water from hot springs and wet-steam wells. American Journal of Science, 264, 685–697

Gíslason, S.R., Heaney, P.J., Oelkers, E.H., and Schott, J. (1997) Kinetic and thermodynamic properties of moganite, a novel silica polymorph. Geochimica et Cosmochimica Acta, 61, 1193–1204.

Goncharov, A.F. and Struzhkin, V.V. (2003) Raman spectroscopy of metals, high temperature superconductors, and related materials under high pressure. Journal of Raman Spectroscopy, 34, 538–548.

Götze, J., Nasdala, L., Kleeberg, R., and Wenzel, M. (1998) Occurrence and distribution of "moganite" in agate/chalcedony: A combined micro-Raman, Rietveld, and cathodoluminescence study. Contributions to Mineralogy and Petrology, 133, 96–105.

Graetsch, H.A. and Brunelli, M. (2005) Incommensurate modulation at 165 °C of intermediate tridymite. Zeitschrift für Kristallographie, 220, 606–613.

Hampton, W.A., White, G.P., Hoskin, P.W.O., Browne, P.R.L., and Rodgers, K.A. (2004) Cinnabar, livingstonite, stibnite and pyrite in Pliocene silica sinter from Northland, New Zealand. Mineralogical Magazine, 68, 191–198.

Heaney, P.J. (1993) A proposed mechanism for the growth of chalcedony. Contributions to Mineralogy and Petrology, 115, 66–74.

——— (1994) Structure and chemistry of the low-pressure silica polymorphs. In P.J. Heaney, C.T. Prewitt, and G.V. Gibbs, Eds., Silica: Physical Behavior, Geochemistry, and Materials Applications, 29, p. 1–40. Reviews in Mineralogy, Mineralogical Society of America, Chantilly, Virginia.

——— (1995) Moganite as an indicator for vanished evaporites: A testament reborn? Journal of Sedimentary Research, A65, 633–638.

Heaney, P.J. and Post, J.E. (1992) The widespread distribution of a novel silica polymorph in microcrystalline quartz varieties. Science, 255, 441–443.

——— (2001) Evidence for an *I2/a* to *Imab* phase transition in the silica polymorph moganite at ~570 K. American Mineralogist, 86, 1358–1366.

Heaney, P.J. and Veblen, D.R. (1991) Observations of the α–β phase transition in quartz: A review of imaging and diffraction studies and some new results. American Mineralogist, 76, 1018–1032.

Herdianita, N.R., Browne, P.R.l., Rodgers, K.A., and Campbell, K.A. (2000) Mineralogical and morphological changes accompanying aging of siliceous sinter and silica residue. Mineralium Deposita, 35, 48–62.

Hopkinson, L., Roberts, S., Herrington R., and Wilkinson, J. (1999) The nature of crystalline silica from the TAG submarine hydrothermal mound, 26°N Mid Atlantic Ridge. Contributions to Mineralogy and Petrology, 137, 342–350.

Kingma, K.J. and Hemley, R.J. (1994) Raman spectroscopic study of microcrystalline silica. American Mineralogist, 79, 269–273.

Landsberg, G. and Mandelstam, L. (1929) Lichtzerstreuung in Kristallen bei hoher Temperatur. Zeitschrift für Physik, 58, 250.

Leadbetter, A.J. and Wright, A.F. (1976) The α–β transition in the cristobalite phases of SiO_2 and $AlPO_4$ I. X-ray studies. Philosophical Magazine, 33, 105–112.

Léger, J.-M. (2001) The high-pressure behavior of the "moganite" polymorph of SiO_2. European Journal of Mineralogy, 13, 351–359.

McKeown, D.A. (2005) Raman spectroscopy and vibrational analyses of albite: From 25 °C through the melting temperature. American Mineralogist, 90, 1506–1517.

McKeown, D.A., Bell, M.I., and Kim, C.C. (1995) Vibrational analysis of dioptase and its puckered six-membered ring. Physics and Chemistry of Minerals, 22, 137.

McMillan, P.F. and Hofmeister, A.M. (1988) Infrared and Raman spectroscopy. In F.C. Hawthorne, Ed., Spectroscopic Methods in Mineralogy and Geology, 18, p. 99–159. Reviews in Mineralogy, Mineralogical Society of America, Chantilly, Virginia.

Miehe, G. and Graetsch, H. (1992) Crystal structure of moganite: A new structure type for silica. European Journal of Mineralogy, 4, 693–706.

Miehe, G., Graetsch, H., Flörke, O.W., and Fuess, H. (1988) Die monokline Kristallstruktur des SiO_2-Minerals Moganit. (Abstr) Zeitschrift für Kristallographie, 182, 183–184.

Moxon, R. and Ríos, S. (2004) Moganite and water content as a function of age in agate: An XRD and thermogravimetric study. European Journal of Mineralogy, 16, 269–278.

Nash, D.J. and Hopkinson, L. (2004) A reconnaissance laser Raman and Fourier transform infrared survey of silcretes from the Kalahari Desert, Botswana. Earth Surface Processes and Landforms, 29, 1541–1558.

Nukui, A., Yamamoto, A., and Nakazawa, H. (1979) Non-integral phase in tridymite. In Cowley, J.M., Cohen, J.B., Salamon, M.B., and Wuensch, B.J., Eds., Modulated Structures-1979. American Institute for Physics Conference Proceedings, 53, 327–329.

Parthasarathy, G., Kunwar, A.C., and Srinivasan, R. (2001) Occurrence of moganite-rich chalcedony in Deccan flood basalts, Killari, Maharashtra, India. European Journal of Mineralogy, 13, 127–134.

Phadke, A.V. and Kshirsagar, L.K. (1986) Thermo-analysis of low cristobalite form Pune, Maharashtra, India: Paragenetic significance. Zeitschrift für Geologische Wissenschaften, 14, 559–567.

Raman, C.V. and Nedungadi, T.M.R. (1940) The α–β transformation of quartz. Nature, 145, 147.

Ríos, S., Salje, E.K.H., and Redfern, S.A.T. (2001) Nanoquartz vs. macroquartz: A study of the α–β phase transition. European Physical Journal B, 20, 75–83.

Rodgers, K.A. and Cressey, G. (2001) The occurrence, detection and significance of moganite (SiO_2) among some silica sinters. Mineralogical Magazine, 65, 157–167.

Rodgers, K.A. and Hampton, W.A. (2003) Laser Raman identification of silica phases comprising microtextural components of sinters. Mineralogical Magazine, 67, 1–13.

Salje, E.K.H. (1992) Hard mode spectroscopy: Experimental studies of structural phase transitions. Phase Transitions, 37, 83–110.

Schmahl, W.W. (1993) Athermal transformation behaviour and thermal hysteresis at the SiO_2--cristobalite phase transition. European Journal of Mineralogy, 5, 377–380.

Schmahl, W.W., Swainson, I.P., Dove, M.T., and Graeme-Barber, A. (1992) Landau free energy and order parameter behaviour of the α/β phase transition in cristobalite. Zeitschrift fur Kristallographie, 201, 125–145.

Scott, J.F. (1968) Evidence of coupling between one and two phonon excitations in quartz. Physical Review Letters, 21, 907–910.

Shapiro, S.M., O'Shea, D.C., and Cummins, H.Z. (1967) Raman scattering study of the α–β transition in quartz. Physical Review Letters, 19, 361–364.

Swainson, I.P., Dove, M.T., and Palmer, D.C. (2003) Infrared and Raman spectroscopy studies of the α–β phase transition in cristobalite. Physics and Chemistry of Minerals, 30, 353–365.

Tucker, M.G., Dove, M.T., and Keen, D.A. (2000) Simultaneous analysis of changes in long-range and short-range structural order at the displacive phase transition in quartz. Journal of Physics: Condensed Matter, 12, L723–L730.

Van Goethem, L., van Landuyt, J., and Amelinckx, S. (1977) The α–β transition in amethyst quartz as studied by electron microscopy and diffraction. Physica Status Solidi, A41, 129–137.

Witke, K., Götze, J., Rößler, DR., Dietrich, D., and Marx, G. (2004) Raman and cathodoluminescence spectroscopic investigations on Permian fossil wood from Chemnitz—A contribution to the study of the permineralization process. Spectrochimica Acta A, 60, 2903–2912.

MANUSCRIPT RECEIVED DECEMBER 8, 2005
MANUSCRIPT ACCEPTED OCTOBER 3, 2006
MANUSCRIPT HANDLED BY JILL PASTERIS